In Situ Ellipsometry Study of the Early Stage of ZnO Atomic Layer Deposition on In 0.53 Ga 0.47 As

Evgeniy V Skopin, Jean-Luc Deschanvres, Hubert Renevier

In situ ellipsometry study of the early stage of ZnO Atomic Layer Deposition on $In_{0.53}Ga_{0.47}As$

Evgeniy V. Skopin[*,1], Jean-Luc Deschanvres[1], and Hubert Renevier[1]

[1] Univ. Grenoble Alpes, CNRS, Institute of Engineering Univ. Grenoble Alpes (Grenoble-INP), LMGP, 38000 Grenoble, France

Key words: Atomic Layer Deposition, ZnO, InGaAs, ellipsometry, oxides, initial growth, growth delay, substrate inhibited growth of type II

[*] Corresponding author: e-mail evgeniy.v.skopin@gmail.com; hubert.renevier@grenoble-inp.fr

We report on the initial stages of ZnO Atomic Layer Deposition (ALD) on $In_{0.53}Ga_{0.47}As$ (InGaAs), studied by monitoring the ZnO film thickness *in situ* with spectroscopic ellipsometry. Using diethylzinc (DEZn) and water, at a substrate temperature equal to 120°C, we found the presence of two different ZnO growth regimes prior to the steady growth: a slow ZnO nucleation on InGaAs, 0.005 nm.cy^{-1} (growth delay), then a substrate inhibited growth of type II. Increasing the DEZn injection time, the growth delay shortened from 30 cycles down to 3 cycles, concomitantly the steady growth rate increased from 0.18 to 0.23 nm.cy^{-1}. The DEZn residence time and pressure increase during the first ALD cycle, allowing to suppress the growth delay, instead, no change is observed when performing the same experiment with water. Atomic Force Microscopy (AFM) images showed that the InGaAs surface roughened after the first cycle with a long DEZn pulse and residence time. The rough surface is likely at the origin of the growth delay elimination.

1 Introduction $In_{x-1}Ga_xAs$ ternary alloy is a semiconductor, with a direct bandgap and high charge carrier mobility, which is widely used in microelectronics [1]. By varying the In/Ga ratio, the face-centered cubic lattice parameter changes from 0.565nm to 0.606nm and the bandgap energy from 1.414eV (x=1) to 0.354eV, respectively (x=0) [2–4]. Thus, this material is widely used in infrared electronics [5]. Thanks to its high carrier mobility, $In_{x-1}Ga_xAs$ can be utilized as a channel material in Metal Oxide Semiconductor Field Effect Transistor (MOSFET) [6,7]. In this case, a possible issue is the metal Fermi level pinning at the Metal-$In_{x-1}Ga_xAs$ interface, leading to an increase of the Metal-Semiconductor contact resistance [8].

However, insertion of an ultra-thin oxide layer in between metal and $In_{x-1}Ga_xAs$ can suppress the metal Fermi level pinning [9]. ZnO is one of the candidates for the ultra-thin oxide layer [10], considering that the thickness of this layer should be close to 1nm in order to optimize the tunneling current flow [11].

One method, which allows controlling of thin film thickness and conformality at the nanometer scale is Atomic Layer Deposition (ALD) [12–14]. Thermal ALD is a Chemical Vapor Deposition (CVD) technique, based on self-limited chemical reactions on the surface heated up to a constant temperature. ALD process consists of sequential cycles. One cycle is a time-sequenced injection of four gases inside the reactor chamber: a metalorganic precursor (DEZn), a purge with inert gas (N_2), an oxidant (H_2O), and a purge. Most generally, thermal ALD provides ideal layer by layer growth with a steady growth rate.

By using synchrotron radiation techniques for monitoring of ZnO ALD on $In_{0.53}Ga_{0.47}As$ (hereinafter InGaAs) [15,16], we put in evidence that the initial ZnO growth on InGaAs is very different from the ideal layer by layer ZnO growth on ZnO. We demonstrated the presence of two successive growth regimes preceding the steady ZnO ALD.

In the present study, we report on the influence of Zn-precursor (diethylzinc) and oxidant (water) injection time or concentration on the ZnO initial growth stages on InGaAs. For monitoring *in situ* the initial stages of growth,

we have implemented spectroscopic ellipsometry [17] on our custom-build reactor, which is used also for X-ray studies [18–20, 15]. Provided that the appropriate model for calculating the thin film optical parameters is known, spectroscopic ellipsometry allows to monitor the thickness as a function of the number of cycles *in situ* and, most importantly, to provide insights into the growth process.

2 Experiment We used commercial InP substrates with 270nm thick InGaAs layer grown by molecular beam epitaxy (III-V Lab, Paris, France). To remove possible oxides on the InGaAs surface [21], the InGaAs substrates were etched in 4M HCl solution for 5 min, then substrates were rinsed in water for 30s, and dried with nitrogen flow. Then, the substrate was immediately uploaded into the ALD reactor chamber and annealed at 200° C for 30min (to evaporate atomic As). After this, we performed ZnO deposition on InGaAs while controlling the thickness by spectroscopic ellipsometry.

To monitor *in situ* the thickness of the ZnO thin film, we used Film Sense FS-1^{TM} Banded Wavelength Ellipsometer and FS-1 software for thickness calculation [22]. The FS-1^{TM} Ellipsometer records the data across 4 discrete wavelengths in the visible spectrum: 465nm (blue), 525nm (green), 580nm (yellow), and 635nm (red). Post growth sample surface morphology was studied *ex situ* by Atomic Force Microscopy (AFM), using a Dimension Icon Bruker^{TM} microscope.

3 Results

3.1 *In situ* thickness monitoring One ZnO ALD cycle contains four steps of sequential gas injections into the reactor chamber: injection of a Zn precursor, a purge of the reactor chamber with inert gas, injection of an oxidant, and again purge. We used $Zn(C_2H_5)_2$ (DEZn) and water as a precursor and oxidant, and nitrogen (N_2) inert gas for purging the reactor. For all samples, the flows of DEZn, water, and N_2 were 5sccm, 2.6sccm, and 1000sccm, respectively. The N_2 purging time after DEZn or water injection was 45s, instead, DEZn and water injection times were varied. The substrate temperature during growth was 120° C for all samples (this temperature is inside the temperature ALD window for DEZn/water ZnO ALD [23,24]). The ZnO thickness was monitored *in situ* by ellipsometry during the ZnO ALD. To calculate the ZnO layer thickness, we modeled the sample by the ZnO(#nm)/InGaAs(270nm)/InP(substrate) stack. Optical coefficients for ZnO, InGaAs layer, and InP substrate were fixed. To determine the refractive indexes *vs.* wavelength λ of the different materials, we used the Cauchy equation [25,22]:

$$n(\lambda[nm]) = n_{633nm} + n_{slope}((\frac{1000}{\lambda})^2 - (\frac{1000}{633})^2), \quad (1)$$

where n_{633nm} is the refractive index for HeNe laser wavelength (633nm); n_{slope} is a constant. The n_{633nm} and n_{slope} values were equal to 3.54 and 0.21 for InP [26], 3.79 and 0.25 for InGaAs [27], and 1.99 and 0.03 for ZnO [28], respectively. The angle of incidence was fixed and equal to 35° with respect to the sample surface normal. The Brewster's angles for InP [26], InGaAs [27], and ZnO [28] are 74.266°, 75.370°, and 63.306°, respectively. ZnO thickness measurements (real-time approximation) were carried out with a 1s integration time. No surface and interface roughnesses were used.

Figure 1 shows an example of the thickness change during one ALD cycle with injection times equal to 80s(DEZn)/45s(N_2)/40s(H_2O)/45s(N_2), respectively. An

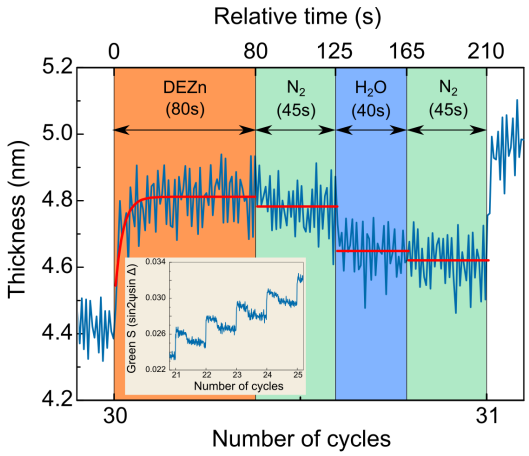

Figure 1 ZnO thickness determined by ellipsometry model as a function of the number of cycles, example for one ALD cycle. One ALD cycle includes DEZn injection (80s, orange region), water injection (40s, blue region), and N_2 purges (45s, green regions). Inset shows raw ellipsometry data of $S = sin2\Psi sin\Delta$ *versus* the number of cycles measured for the same sample.

example of raw data S ($S = sin2\Psi sin\Delta$) *vs.* number of cycles for this sample is shown in the inset of Figure 1 (Ψ and Δ are the amplitude ratio and phase angle, determined as $R_p/R_s = tan\Psi e^{i\Delta}$, where R_p and R_s are the complex Fresnel reflection coefficients for p- and s-polarized light [17]). As Figure 1 shows, the thickness noise amplitude is about 0.05nm (the noise level decreases, for instance, by increasing acquisition time). When the DEZn injection begins, the layer thickness abruptly increases and then reaches a constant value (orange area in Figure 1). For the experimental data visualization, the experimental thicknesses were fitted by a sigmoidal function in the DEZn injection area (red line). During N_2 purging after the DEZn injection, a slight thickness decrease is observed (green left area, the red lines correspond to the average thickness). When water is injected, a clear thickness decrease is observed (blue area). During N_2 purge after water injection, the grown layer thickness slightly decreases (green area on the right).

Figure 2(a) shows the measured thickness *vs.* cycle number during ZnO ALD for a sample grown with injection times equal to 5s(DEZn)/45s(N_2)/10s(H_2O)/45s(N_2), respectively. At the beginning of growth (regime I), a thickness jump is observed at the first cycle, then the thickness almost does not change, the average thickness slowly increases (see zoom inset, blue oval; gray line shows the average thickness for every cycle). During this growth delay, the thickness steps are not visible, then the thickness steps become visible and the step height changes at higher cycle numbers (regime II, see inset, red oval). The growth rate in regime II is not constant, a thickness S-shape curve is observed [29]. At last, the thickness increases linearly and the growth rate becomes constant (regime III, the step height is constant, green oval on Fig.2(a)).

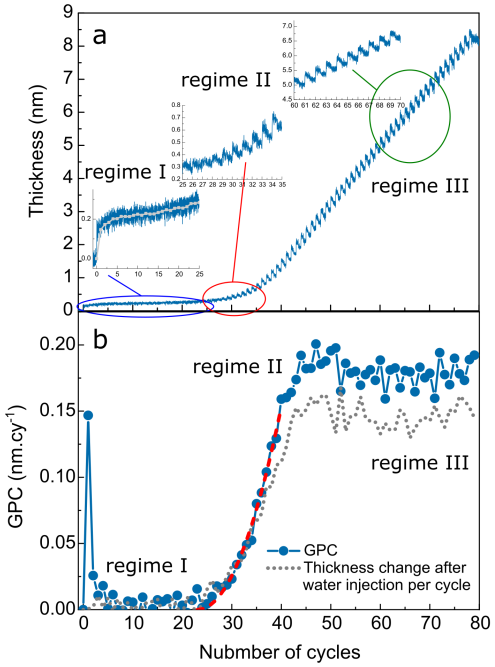

Figure 2 ZnO Thickness (a) and GPC (b) as a function of the number of cycles measured for a sample grown with injection times equal to 5s(DEZn)/45s(N_2)/10s(H_2O)/45s(N_2). Growth includes different regimes: growth delay (regime I), substrate inhibited growth of type II (regime II), and steady growth (regime III). The red dash line is a parabolic fit. Gray dot line represents a difference between the thickness after DEZn injection and after water injection for the chosen cycle as a function of the number of cycles.

Figure 2(b) shows the experimental growth per cycle (GPC) values as function of the number of cycles. We calculated GPC for cycle n as the difference in thickness for cycle n and thickness for cycle $(n-1)$. The thickness values for cycle n and $(n-1)$ are the average thicknesses during N_2 purge after water injection (see Figure 1).

During regime I, the GPC is constant and almost zero, except for cycle 1 (GPC is about 0.15nm.cy^{-1}). Then, in regime II the GPC shows the characteristic substrate inhibited growth of type II [29], that is the GPC shows a parabolic increase, reaches a maximum, and then decreases to reach a constant value. In regime III (steady growth state) the GPC is constant.

Assuming that the GPC(n) curve in regime II has a parabolic increase in the beginning, we fitted the data with function $A(n-n_{delay})^2$, where n_{delay} is the number of ALD cycles at which the parabolic GPC begins [15], and A is a scale factor. The parabolic GPC fit curve (red dash line) gives the number $n_{delay} = 22$ cycles for the corresponding sample.

As shown in Figure 1, the layer thickness decreases after water injection, instead, the thickness obtained after the DEZn injection is barely affected. Figure 2(b) (gray dotted line) shows the difference between the thickness after DEZn injection and the thickness after water injection for each cycle. Experimental layer thickness after DEZn or water injection was calculated with the values recorded inside the N_2 purge areas (see Fig. 1).

Figure 2(b) shows that this function has a value close to zero (including the first ALD cycle) in the regime I. Then in regime II, this function grows proportionally to the GPC function. In regime III, this function reaches a constant value ($\approx$0.15nm.cy^{-1}). This means that after the water pulse the thickness decrease (likely due to C_2H_5 ligand effusion) is constant during the steady growth state.

To study how the DEZn and water concentrations modify growth, i.e. the growth delay and steady state growth (GPC), we grew a series of samples by varying the DEZn injection time.

3.2 DEZn concentration *vs.* growth delay In a previous study [15], we demonstrated the effect of water concentration (by varying the water flow) on the initial stages of growth, by monitoring Zn X-ray Fluorescence (XRF) signal during ZnO growth on InGaAs. We showed the possibility to decrease the growth delay (number of cycles in regime I, see Fig. 2), at higher water flow.

Here, we report on the influence of DEZn molecules concentration on the growth delay. We monitored the growth by *in situ* ellipsometry for a series of samples with different DEZn injection times. The injection times for this series were equal to #s(DEZn), 45s(N_2), 40s(H_2O) and 45s(N_2). DEZn injection time # from one sample to another was 1s, 2s, 5s, 10s, 20s, 40s, and 80s. Other deposition parameters were fixed as described in Section 3.1.

Figure S1 (see supplementary information) shows the ZnO thickness (a) and corresponding GPC (b) as a function of the number of cycles for different DEZn injection times (different samples).

All recorded GPC curves exhibit the same shape: a growth delay (regime I), substrate inhibited growth of type II (regime II), and steady growth (constant GPC, regime

III). Figure S1 shows that the growth delay (regime I) is shortened while increasing the DEZn injection time. Figure 3 shows steady growth GPC (a) and n_{delay} (b) as a function of DEZn injection time. The steady GPC increases for

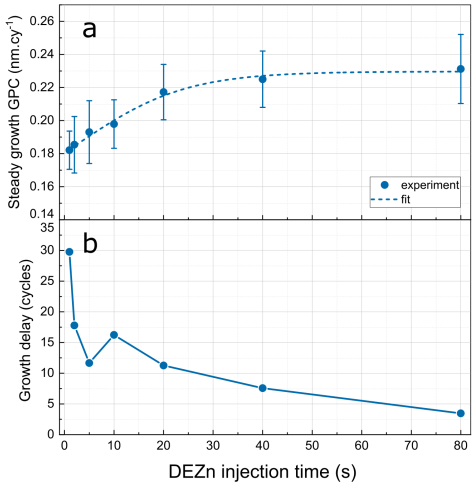

Figure 3 Steady growth GPC (a) and growth delay n_{delay} (b) as functiuons of DEZn injection time. Other growth parameters were fixed.

higher DEZn injection times from 0.18nm.cy^{-1} (for 1s of DEZn injection) to 0.23nm.cy^{-1} (for 80s of DEZn injection). First, there is a significant GPC increase for the range 1s-20s (0.18nm.cy^{-1}-0.22nm.cy^{-1}), and then an asymptotic GPC increase for the range 20s-80s (0.22nm.cy^{-1}-0.23nm.cy^{-1}). The steady GPC reaches a plateau for a DEZn injection time beyond 20s.

The opposite trend is observed for n_{delay}(Fig. 3(b)). n_{delay} decreases when increasing DEZn injection times from 30 cycles (1s of DEZn injection) to 3 cycles (80s of DEZn injection). For 20s-80s DEZn injection times, when steady GPC is almost constant (0.22nm.cy^{-1}-0.23nm.cy^{-1}), n_{delay} decreases from 11 cycles to 3 cycles. It is clear that the increase of DEZn injection time (increasing the number of DEZn molecules inside the reaction chamber) leads to the decrease of the growth delay and to have about the same steady growth rate.

3.3 Long water/DEZn pulse during cycle 1 As reported in Section 3.2, an increase of water or DEZn molecules concentration during the precursor pulse, decreases n_{delay}. The change of substrate surface functionalization after the first cycle can lead to different ZnO growth behavior. To check that in the case of ZnO ALD on InGaAs, we monitored thickness *in situ* while injecting a long pulse of water or DEZn into the reactor at the first cycle. The main growth parameters were fixed as described in Section 1, for cycles 2-50, DEZn (resp. water) injection time was 5 s (resp. 40 s).

Regarding the long water pulse cycle (inset of Figure 4(a)), as usual, DEZn was first injected into the reactor for 5s. Then, the reactor was purged with N_2 during 45s.

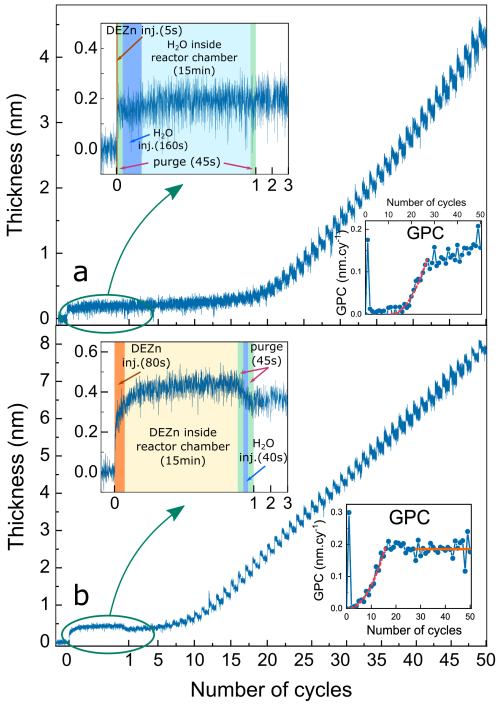

Figure 4 Long water (a) and DEZn (b) injection during the first cycle: thickness as a function of the number of cycles. Left insets: description of gas injections during first ALD cycle. Right insets: GPC as a function of the number of cycles with parabolic fits (n_{delay} is 11 cycles (a) or 0 cycles (b) for long water or DEZn injection during the first ALD cycle).

After the purge, water vapor was injected into the reactor chamber during 160s (up to 2mbar inside the reactor chamber). Water was kept in the closed reactor chamber for 15 min, then the reactor was purged with N_2 for 45s. For cycles 2-50, the injection times for DEZn/N_2/H_2O/N_2 were 5s/45s/40s/45s, respectively.

Figure 4(a) shows the thickness and GPC as functions of the number of cycles measured for a long first-cycle water injection time. Despite this long time for the water to react, a growth delay is still present, n_{delay} is about 11 cycles.

A similar experiment was performed with a long DEZn pulse at the first cycle (see inset of Figure 4(b)). A 5sccm flow of DEZn was injected inside the closed reactor chamber during the 80s (to reach a 2mbar pressure inside the reactor chamber). Then, DEZn molecules were kept inside the reactor chamber for 15min to react. Then, DEZn was purged with nitrogen for 45s, water was injected for 40s, and the reactor was purged again for 45s. For cycles 2-50, injection times were 5s/45s/40s/45s for DEZn/N_2/H_2O/N_2, respectively.

Unlike long water pulse, a long DEZn pulse causes the suppression of the growth delay (see right inset of Fig-

ure 4(b), n_{delay} is close to 0 cycles). Even though a less amount of DEZn (DEZn injection time is 5s) is injected during cycles 2-50, there is no growth delay, the growth starts immediately with regime II.

To check a possible change of surface morphology, we performed AFM of the InGaAs surface after HCl cleaning (Figure 5(a)) and 1 ZnO ALD cycle comprising a long DEZn pulse (Figure 5(b)). The dotted lines on the AFM

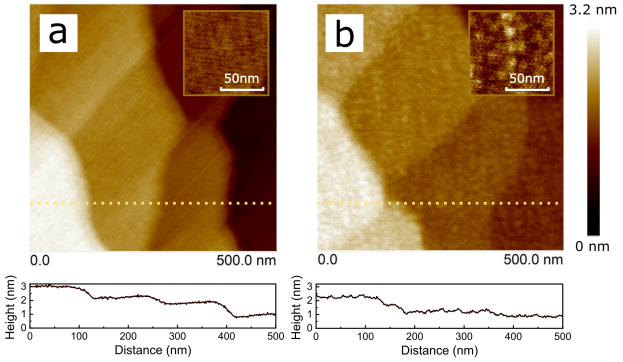

Figure 5 Atomic Force Microscopy (AFM) images obtained for InGaAs surface after HCl treatment (a) and InGaAs surface after one ALD cycle with a long DEZn injection (b). Yellow dotted lines on the images shows the positions of the cross lines (corresponding cross lines shown below the AFM images).

images indicate the position of surface cross lines, shown under the AFM images. InGaAs surface is presented by atomically flat terraces, the InGaAs roughness (RMS) on the terraces is about 0.05nm, and the RMS of the terraces is 0.3nm. The plot above Fig. 5(a) shows the cross line of the InGaAs terraces after HCl cleaning. After 1 ZnO ALD cycle, including the long DEZn pulse, surface roughness (RMS) increases up to 0.09nm (see Fig. 5(b)).

4 Discussion ZnO growth on either InGaAs or ZnO surface is very different [15,16]. ZnO ALD on ZnO has been the subject of experimental works [30], and more recently of DFT and Monte Carlo simulations [31–36]. Besides, ZnO surface reactivity, which depends on the surface polarity and reconstruction, has been studied [37, 38]. In the present study, we focused on the control of the growth delay during ZnO ALD on InGaAs, by varying the injection time of precursors. During the growth delay (regime I, inset of Fig. 2(a)), the GPC is 30-50 times smaller (about 0.005nm.cy^{-1}) than the steady growth GPC (0.18-0.23nm.cy^{-1}, at a substrate temperature equal to 120° C). However, the slight thickness increase is a clear indication of the presence of chemical reactions occurring on the InGaAs surface.

In Figure 2 we observe that the GPC for the first ALD cycle is higher than for cycles in the range [2-n$_{delay}$]. During the first ALD cycles, DEZn reacts with active surface sites, present on InGaAs surface, and leads to higher GPC value than those observed in the next cycles. Thus, we hypothesized that a long time left for water or DEZn to react (or higher concentration of water or DEZn) could increase the number of active surface sites available for the next cycles, and could shorten the growth delay.

We found that after a long water injection time at the first cycle (see Section 3.3, Fig. 4(a)), n$_{delay}$ is still 12 cycles, the same value as observed in the case of usual water injection time (all other parameters being identical). Evidently, a long interaction with water does not lead to a significant increase of active surface sites on InGaAs (OH-groups, water molecules) for a reaction with DEZn.

Regarding the DEZn effect, we observed that by increasing DEZn pulse duration (*i.e.* the DEZn concentration inside the closed reactor chamber), the growth delay is shortened. Besides, by increasing the DEZn injection time from 20s to 80s, the steady growth GPC values are almost the same (0.22-0.23nm.cy^{-1}, Fig. 3(a)), whereas the number of cycles, n$_{delay}$, decreases from 11 cycles down to 3 cycles. The same effect was observed for a long DEZn injection during the first cycle, n$_{delay}$ became close to 0 cycles (inset of Fig. 4(b)). Both ways for DEZn injection (80s of DEZn injection every cycle or long DEZn injection during the first cycle) leads to the disappearance of regime I. This means that a long interaction of DEZn with InGaAs surface renders InGaAs surface more reactive.

AFM image (Fig. 5), obtained after one ALD cycle comprising a long DEZn injection, shows that the morphology of InGaAs surface has changed in comparison with InGaAs cleaned surface. Small nuclei or islands have appeared.

One possible process during the long DEZn injection can be a reaction between monoethylzinc (MEZn) on the InGaAs sufrace with DEZn molecule. Weckman *et al.* [31] demonstrated that this type of reaction can lead to the formation of additional bare Zn atoms and products of the reaction (organic molecules). Then, this Zn atom can adsorb more water molecules, leading to a growth rate increase.

More investigations are needed to determine the chemical reactions at play in between DEZn, water, and InGaAs surface at the early stage of growth of ZnO by ALD.

Acknowledgements E.V. Skopin was supported by ANR project ANR-18-CE09-0031-03 and the LabEx Minos ANR-10-LABX-55-01. Financial support by the Centre of Excellence of Multifunctional Architectured Materials (Labex CEMAM) ANR-10-LABX-44-01 for implementing the ellipsometer is gratefully acknowledged. We acknowledge D. De Barros for engineering assistance. We thank laboratory of Science et Ingénierie des Matériaux et Procédés (SIMAP, Grenoble-INP, Grenoble (France)) for technical assistance.

References

[1] J. A. Del Alamo, Nature **479**(7373), 317 (2011).
[2] H. Ishikawa, Applied physics letters **63**(6), 712–714 (1993).
[3] J. C. Woolley, M. B. Thomas, and A. G. Thompson, Canadian Journal of Physics **46**(2), 157–159 (1968).

[4] J. W. Wagner, Journal of The Electrochemical Society **117**(9), 1193–1196 (1970).
[5] M. Heyns and W. Tsai, Mrs bulletin **34**(7), 485–492 (2009).
[6] A. Sonnet, R. Galatage, P. Hurley, E. Pelucchi, K. Thomas, A. Gocalinska, J. Huang, N. Goel, G. Bersuker, W. Kirk et al., Microelectronic Engineering **88**(7), 1083–1086 (2011).
[7] M. Paladugu, C. Merckling, R. Loo, O. Richard, H. Bender, J. Dekoster, W. Vandervorst, M. Caymax, and M. Heyns, Crystal Growth & Design **12**(10), 4696–4702 (2012).
[8] J. Robertson, Journal of Vacuum Science & Technology A: Vacuum, Surfaces, and Films **31**(5), 050821 (2013).
[9] D. Connelly, C. Faulkner, D. Grupp, and J. Harris, IEEE Transactions on Nanotechnology **3**(1), 98–104 (2004).
[10] M. H. Liao and C. Lien, AIP Advances **5**(5), 057117 (2015).
[11] A. Agrawal, N. Shukla, K. Ahmed, and S. Datta, Applied Physics Letters **101**(4), 042108 (2012).
[12] P. O. Oviroh, R. Akbarzadeh, D. Pan, R. A. M. Coetzee, and T. C. Jen, Science and technology of advanced materials **20**(1), 465–496 (2019).
[13] S. M. George, Chemical reviews **110**(1), 111–131 (2009).
[14] V. Miikkulainen, M. Leskelä, M. Ritala, and R. L. Puurunen, Journal of Applied Physics **113**(2), 2 (2013).
[15] E. V. Skopin, L. Rapenne, H. Roussel, J. L. Deschanvres, E. Blanquet, G. Ciatto, D. D. Fong, M. I. Richard, and H. Renevier, Nanoscale **10**, 11585–11596 (2018).
[16] E. V. Skopin, L. Rapenne, J. L. Deschanvres, E. Blanquet, G. Ciatto, L. Pithan, D. D. Fong, M. I. Richard, and H. Renevier, submitted (2019).
[17] E. Langereis, S. Heil, H. Knoops, W. Keuning, M. Van de Sanden, and W. Kessels, Journal of Physics D: Applied Physics **42**(7), 073001 (2009).
[18] R. Boichot, L. Tian, M. I. Richard, A. Crisci, A. Chaker, V. Cantelli, S. Coindeau, S. Lay, T. Ouled, C. Guichet et al., Chemistry of Materials **28**(2), 592–600 (2016).
[19] M. H. Chu, L. Tian, A. Chaker, V. Cantelli, T. Ouled, R. Boichot, A. Crisci, S. Lay, M. I. Richard, O. Thomas et al., Crystal Growth & Design **16**(9), 5339–5348 (2016).
[20] M. H. Chu, L. Tian, A. Chaker, E. Skopin, V. Cantelli, T. Ouled, R. Boichot, A. Crisci, S. Lay, M. I. Richard et al., Journal of Electronic Materials **46**(6), 3512–3517 (2017).
[21] Y. Sun, P. Pianetta, P. T. Chen, M. Kobayashi, Y. Nishi, N. Goel, M. Garner, and W. Tsai, Applied Physics Letters **93**(19), 194103 (2008).
[22] FilmSenceLLC, FS-1 manual2015).
[23] E. Guziewicz, I. Kowalik, M. Godlewski, K. Kopalko, V. Osinniy, A. Wójcik, S. Yatsunenko, E. Łusakowska, W. Paszkowicz, and M. Guziewicz, Journal of Applied Physics **103**(3), 033515 (2008).
[24] Z. Gao, F. Wu, Y. Myung, R. Fei, R. Kanjolia, L. Yang, and P. Banerjee, Journal of Vacuum Science & Technology A: Vacuum, Surfaces, and Films **34**(1), 01A143 (2016).
[25] H. Fujiwara, Spectroscopic ellipsometry: principles and applications (John Wiley & Sons, 2007).
[26] D. E. Aspnes and A. Studna, Physical review B **27**(2), 985 (1983).
[27] S. Adachi, Journal of Applied Physics **66**(12), 6030–6040 (1989).
[28] W. Bond, Journal of Applied Physics **36**(5), 1674–1677 (1965).
[29] R. L. Puurunen and W. Vandervorst, Journal of Applied Physics **96**(12), 7686–7695 (2004).
[30] T. Tynell and M. Karppinen, Semiconductor Science and Technology **29**(4), 043001 (2014).
[31] T. Weckman and K. Laasonen, The Journal of Physical Chemistry C **120**(38), 21460–21471 (2016).
[32] T. Weckman, M. Shirazi, S. D. Elliott, and K. Laasonen, The Journal of Physical Chemistry C **122**(47), 27044–27058 (2018).
[33] T. Weckman and K. Laasonen, The Journal of Physical Chemistry C **122**(14), 7685–7694 (2018).
[34] A. Afshar and K. C. Cadien, Applied Physics Letters **103**(25), 251906 (2013).
[35] S. Patwardhan, D. H. Cao, G. C. Schatz, and A. B. Martinson, ACS Applied Energy Materials (2019).
[36] S. Kim, S. Lee, S. Y. Ham, D. H. Ko, S. Shin, Z. Jin, and Y. S. Min, Applied Surface Science **469**, 804–810 (2019).
[37] S. Chamberlin, C. Hirschmugl, S. King, H. Poon, and D. Saldin, Physical Review B **84**(7), 075437 (2011).
[38] S. King, S. Parihar, K. Pradhan, H. T. Johnson-Steigelman, and P. Lyman, Surface Science **602**(22), L131–L134 (2008).

Graphical Table of Contents

GTOC image:

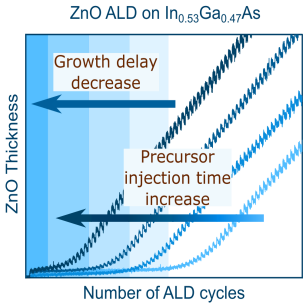

Your article will be published with a Graphical Abstract in the table of contents. Please send a suggestion for an image (preferably full colour, size 4 cm x 4 cm). It may be specifically designed for the purpose, but should not show too many details or consist of several parts. Enclose a short descriptive and popular text on the general aim and value of your paper which may serve as an 'appetizer' for the readers (40–70 words, not a Figure caption, not the abstract text).